THE JOURNAL OF PHYSICAL CHEMISTRY C
A JOURNAL OF THE AMERICAN CHEMICAL SOCIETY

pubs.acs.org/JPCC

Perspective

Uncovering Transport Mechanisms in Perovskite Materials and Devices with Recombination-Induced Action Spectroscopies

Meredith G. McNamee,[#] Zhenyu Ouyang,[#] Liang Yan, Zijian Gan, Ninghao Zhou, Olivia F. Williams, Wei You, and Andrew M. Moran*

Cite This: *J. Phys. Chem. C* 2023, 127, 2782−2791

Read Online

ACCESS | Metrics & More | Article Recommendations | Supporting Information

ABSTRACT: Although valuable insights are derived from conventional spectroscopic approaches, the understanding of a photovoltaic device's operation mechanisms can be limited in *ex situ* measurements. For example, the signals measured in transient absorption experiments reflect the concentrations and extinction coefficients of all photoexcited species in a material regardless of functional relevance. Elimination of such ambiguities has motivated the development of various "action spectroscopy" techniques in which the response of a photovoltaic device to a sequence of laser pulses is directly detected. The class of action spectroscopies described in this Perspective leverages recombination-induced nonlinearities to distinguish lossy (fluorescence) and productive (photocurrent) processes within the active layers of photovoltaic cells. Although recombination processes are problematic in alternate approaches for conducting action spectroscopies, our experiments show that this type of nonlinearity can be exploited to reveal transport mechanisms on nanosecond time scales. Applications to mixtures of layered perovskite quantum wells are presented to demonstrate signatures of energy funneling and long-range carrier drift in photovoltaic devices.

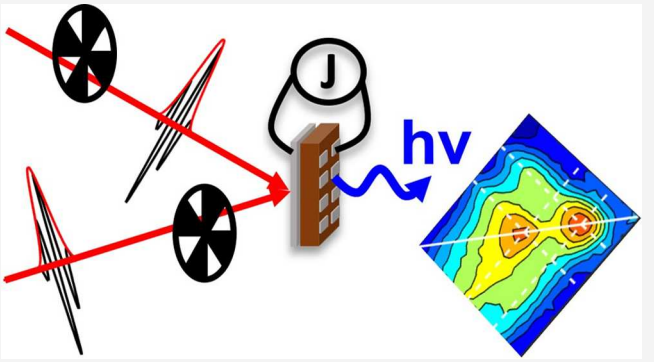

INTRODUCTION

The development of two-dimensional (2D) Fourier transform electronic spectroscopies has enabled physical insights into processes ranging from solvation in liquids to light harvesting in photosynthesis.[1−3] Knowledge of sub-ps dynamics can be gathered by detecting coherent light emission in conventional spectroscopic approaches; however, the signals are weighted by the concentrations and extinction coefficients of all photoexcited species in the focal volume regardless of their functional significances. For example, due to their neutral charges, excitons do not drift in response to a built-in potential within a photovoltaic cell but may produce spectroscopic signals with greater magnitudes than coexisting electrons and holes. To reduce ambiguities in experimental interpretations, action spectroscopies have been developed in which spontaneous processes such as the fluorescence and photocurrent generated by a device are measured instead of coherent light emission. Nonlinear fluorescence action spectroscopies have been employed in studies of molecular aggregates exhibiting Frenkel exciton electronic structure.[4−17] In addition, nonlinear photocurrent spectroscopies have been used to uncover ultrafast dynamics (e.g., exciton dissociation, charge transfer)[18−25] and long-range drift in photovoltaic cells.[26−30] These earlier works demonstrate that spontaneous processes can be exploited in creative ways to characterize photoinduced dynamics.

Higher order perturbative responses have been targeted in most previous applications of action spectroscopies;[4−7,9,10,12−25,31] however, alternate signal generation mechanisms can be advantageous depending on the material and desired information.[26−30] For example, two- and four-pulse implementations of nonlinear action spectroscopies are compared in Figure 1. In Figure 1a, a sequence of four laser pulses with experimentally controlled phases (Ω_j) is used to isolate signal components resembling the ground state bleach, excited state emission, and excited state absorption responses present in conventional transient absorption and 2D electronic spectroscopies.[32] The first and second pair of laser pulses accomplish the "pump" and "probe" processes in this type of technique. Such four-pulse, Fourier transform methods are well-suited for studies of femtosecond light harvesting and/or charge transfer dynamics because the time resolution is limited

Received: December 18, 2022
Revised: January 23, 2023
Published: February 2, 2023

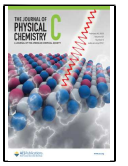

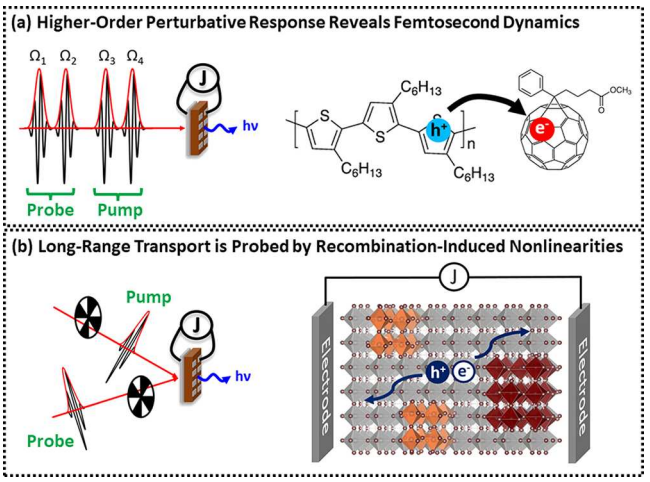

Figure 1. Functionally significant dynamics are selectively measured with nonlinear action spectroscopies applied to materials and photovoltaic devices. Experimental approaches may target either (a) higher order perturbative or (b) recombination-induced signal generation mechanisms. Laser pulse width-limited time resolution is achieved with phase cycling and/or phase modulation methods when higher order perturbative responses are probed, thereby enabling studies of femtosecond energy and charge transfer processes. Alternatively, recombination-induced nonlinearities can be exploited for studies of slower, long-range transport dynamics in devices and semiconductor films.

by the laser pulse durations. Like pump−probe methods, Fourier transform action spectroscopies can also be to study processes on longer time scales by introducing a delay between the two pulse pairs.

By contrast, the nonlinear response detected with the two-pulse approach presented in Figure 1b originates in recombination processes involving species photoexcited by separate laser pulses.[29] Consequently, the time resolution depends on the nature of the material, laser intensity, and recombination mechanism. For example, the authors of the present work have leveraged two-body recombination mechanisms[33] to extract time-of-flight information from photovoltaic cells based on perovskite materials.[27−30] Thus, although recombination processes are regarded as experimental artifacts in Fourier transform approaches,[9,11,12,16,34] they can be leveraged for studies of transport mechanisms on nanosecond time scales. Whereas theoretical descriptions of four-pulse Fourier transform spectroscopies have been discussed in several recent publications,[9,12,35] signal generation mechanisms associated with recombination-induced nonlinear action spectroscopies are at an earlier stage of development.[29,30] In this Perspective, we aim to clarify the potential of such two-pulse action spectroscopies for studies of long-range transport mechanisms in devices and semiconductor materials.

SIGNALS GENERATION MECHANISMS IN NONLINEAR ACTION SPECTROSCOPIES

Higher order perturbative and recombination-induced nonlinearities are distinguished with energy level diagrams in Figure 2 to clarify the signal generation mechanisms associated with the techniques represented in Figure 1. In Figure 2a, we present diagrams in which the pulse-pairs are represented with single arrows to capture essential aspects of the field-matter interactions as a detailed theoretical description of Fourier transform 2D action spectroscopy is beyond the scope of the present work. Although we have simplified the physical picture, it can be understood that the first and second pulse-pairs to arrive at the sample in Figure 1a correspond to "pump" and "probe" events because two field−matter interactions are required to change the population of an electronic state in this type of experiment.[32] The probe laser pulses interact with a photoexcited species in a higher order perturbative response, thereby enabling spectroscopic transitions between excited states. For example, the energy level diagram shown in Figure 2a represents an excited state absorption process. Conventional pump−probe experiments correspond to third-order in time-

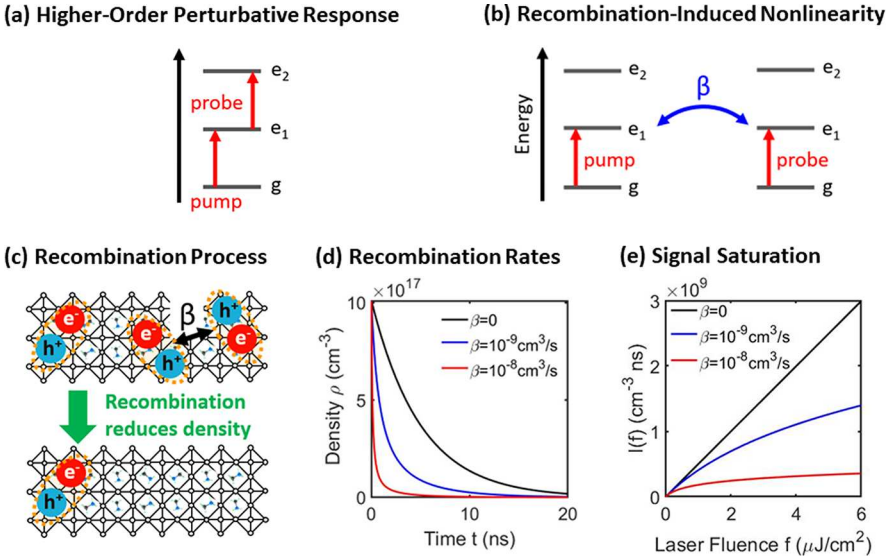

Figure 2. Technical distinctions between alternate signal generation mechanisms. (a) The probe pulse interacts with a photoexcited species in a higher order perturbative process. (b) In contrast, each laser pulse interacts with the equilibrium system in techniques that target recombination-induced nonlinearities (β is a two-body recombination coefficient). (c) For example, exciton−exciton annihilation saturates the density of photoexcitations in layered perovskite materials. (d) Recombination time scales decrease as the magnitudes of two-body coefficients increase. (e) The integrated densities of photoexcited species scale nonlinearly with the laser fluences.

https://doi.org/10.1021/acs.jpcc.2c08851
J. Phys. Chem. C 2023, 127, 2782−2791

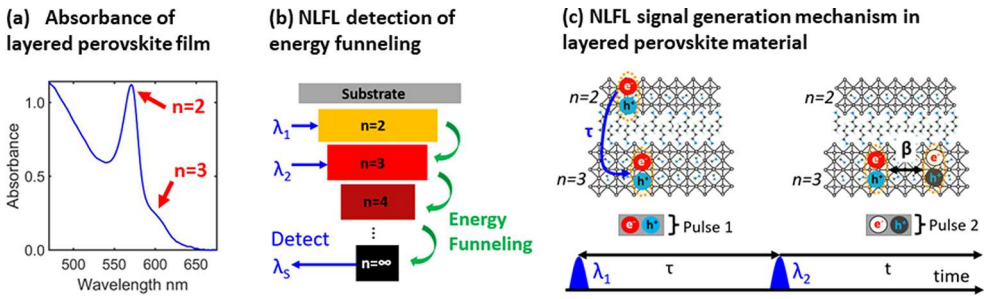

Figure 3. Nonlinear fluorescence spectroscopy has been applied to mixtures of layered perovskite quantum wells in recent literature. (a) Absorbance spectrum of a layered perovskite film exhibits exciton peaks associated with quantum wells composed of 2 and 3 layers of lead-iodide octahedra. (b) Nonlinear fluorescence experiments reveal energy funneling processes on time scales of 100s of ps. (c) The first laser pulse initiates energy funneling, whereas the second pulse probes transient populations of quantum wells through exciton−exciton annihilation processes.

dependent perturbation theory,[32] whereas the class of 2D action spectroscopies depicted in Figure 1a involves a fourth-order perturbative response because the signal is spontaneously generated after the second pair of laser pulses arrives at the sample. Theoretical treatments of such higher order perturbative responses have been presented elsewhere.[9,12,22,24,35]

By contrast, the pump and probe laser pulses are both absorbed by the equilibrium system in the signal generation mechanism associated with the technique in Figure 1b. Consequently, resonances between excited states cannot contribute to the response, and the time resolution of the technique depends on the rate at which recombination processes saturate the fluorescence or photocurrent produced by a device. Recombination-induced nonlinearities are seen as a nuisance in studies of molecular aggregates because they are incapable of resolving femtosecond energy transfer dynamics and do not provide insights into biexciton electronic structure. The type of process shown in Figure 2b, which has been referred to as incoherent and/or a mixture of linear responses,[8,9,11,12,16,34] is not regarded as a "true nonlinear signal" in studies of femtosecond dynamics;[9,36] however, this signal generation mechanism can be leveraged in studies of slower, long-range processes in materials and devices. Notably, the nonlinearity represented in Figure 2b is fundamentally different from a cascade of lower-order responses, such as those observed in off-resonant 2D Raman spectroscopies[37,38] because it provides dynamical information that is not available when a material absorbs a single laser pulse. For example, recent studies of layered perovskite systems demonstrate that recombination-induced nonlinearities can be exploited to resolve energy and charge funneling dynamics in layered perovskite systems on time scales of 100s of ps.[15,26−29]

Recombination processes saturate the total amount of photocurrent or fluorescence collected from a material as the laser intensity increases (e.g., layered perovskite quantum wells in Figure 2c). To illustrate the relevant time scales, we compute dynamics in the density of a photoexcited species subject to a two-body recombination process using

$$\frac{d\rho(t,f)}{dt} = -\gamma\rho(t,f) - \beta\rho^2(t,f) \tag{1}$$

where f is the laser fluence, γ^{-1} is a lifetime, and β is a two-body recombination coefficient. To approximate the behaviors of layered perovskite systems, the lifetime is set equal to 5 ns, whereas the two-body recombination coefficient ranges from 10^{-8}−10^{-9} cm^3/s in Figure 2d,e.[39−45] In these calculations, the initial concentration of photoexcitations is estimated by averaging the densities at the two interfaces of a thin film,

$$\rho(0,f) = \frac{\alpha f}{2}[1 + \exp(-\alpha l)] \tag{2}$$

where α is the absorbance coefficient (4 μm^{-1}) and l is the film thickness (100 nm). The carrier density is also time-integrated in Figure 2e to characterize the magnitude of the nonlinearity:

$$I(f) = \int_0^\infty \rho(t,f)\, dt \tag{3}$$

Beginning with initial values of 10^{18} cm^{-3}, the densities in Figure 2d decay by 50% at times of 3.5, 0.8, and 0.1 ns when β is set equal to 0, 10^{-9}, and 10^{-8} cm^3/s, respectively. These dynamics reflect the time scales and efficiencies of the probing processes associated with recombination-induced nonlinearities. For the class of action spectroscopies depicted in Figure 1b, the delay time between laser pulses is known with pulse duration-limited precision, whereas the signal is subsequently generated as recombination processes accumulate and saturate the fluorescence or photocurrent produced by a device. In experiments conducted on layered perovskites, we have observed dynamics on the 100 ps time scale and shown that the same energy funneling time constants can be obtained with conventional femtosecond transient absorption and nonlinear fluorescence action spectroscopies.[15,26,39]

In Figure 2e, the magnitude of the nonlinearity is characterized by time-integrating the densities with β equal to 0, 10^{-9}, and 10^{-8} cm^3/s (see eq 3). The nonlinear dependence of $I(f)$ on the laser fluence represents the signal generation mechanism associated with the technique represented in Figure 1b. These experiments are conducted by measuring the total amounts of photocurrent or fluorescence generated with the individual laser pulses, S_1 and S_2.[26] The signal measured with the sample exposed to both laser pulses, $S_{1+2}(\tau)$, additionally depends on the experimentally controlled delay time, τ. The nonlinearity induced by recombination processes involving species photoexcited by separate laser pulses is then obtained by evaluating the linear combination, $S_{Action}(\tau) = S_{1+2}(\tau) - S_1 - S_2 + S_0$, where S_0 is the "background" measured when the sample is not exposed to light. For example, with $\beta = 10^{-9}$ cm^3/s, the values of $I(f)$ computed with laser fluences of 1 and 2 μJ/cm^2 are 1.0×10^{19} and 1.7×10^{19} cm^{-3}·ns, respectively. Thus, the magnitude of the response corresponds to a saturation percentage of ϕ = 14%, where ϕ is given by

https://doi.org/10.1021/acs.jpcc.2c08851
J. Phys. Chem. C 2023, 127, 2782−2791

$$\phi = \frac{2I(f) - I(2f)}{2I(f)} \tag{4}$$

Because the magnitude of $S_{\mathrm{Action}}(\tau)$ reflects the curvature of $I(f)$, the signals must decay as the concentrations of species photoexcited by the first laser pulse decrease in τ.

ENERGY FUNNELING DYNAMICS IN LAYERED PEROVSKITE SYSTEMS REVEALED BY NONLINEAR FLUORESCENCE SPECTROSCOPY

As shown in Figure 1b, the photocurrent and fluorescence generated by a photovoltaic cell can be measured in tandem to distinguish productive and lossy relaxation mechanisms.[26] We have presented detailed simulations of nonlinear photocurrent experiments in recent works[29,30] but have not applied this type of model to nonlinear fluorescence (NLFL) spectroscopy. Therefore, to clarify the information provided by recombination-induced nonlinearities, we next compare experimental and simulated NLFL signatures of energy funneling for a mixture of layered perovskite quantum wells. The components of the material are described by the chemical formula $BA_2MA_{n-1}Pb_nI_{3n+1}$, where BA is butylammonium, MA is methylammonium, and the subscript n represents the number of stacked lead-iodide octahedra within the quantum wells.[46,47] For example, quantum wells with n = 2 and 3 exhibit exciton peaks at 570 and 610 nm in the linear absorbance spectrum shown in Figure 3a. Light absorption initiates energy funneling processes wherein excitations transfer to successively thicker quantum wells until they reach a quasi-3D phase of $MAPbI_3$-like material.[26,39,48−54] In our experiments, the two color-tunable laser pulses, λ_1 and λ_2, target the initial and intermediate locations of the electronic excitations in the 500−650 nm wavelength range, whereas fluorescence is detected at λ_S = 725 nm to make the signal specific to energy funneling processes terminating in the quasi-3D layer ($n = \infty$ in Figure 3b).

In Figure 3c, we illustrate the processes that occur during the experimentally controlled delay time, τ, and the detection time, t. The first laser pulse initiates an energy transfer process between the n = 2 and 3 quantum wells, which are most concentrated in the system considered in Figure 3a. The time constant for this energy transfer process is 100−1000 ps depending on the distribution of proximities between quantum wells arising from the fabrication conditions.[50,39,54] Notably, the NLFL signals are sensitive to the overall time scale in which excitons accumulate in the n = 3 quantum wells and reflect exciton diffusion when the systems are not in close proximity due to differences in concentrations and film heterogeneity. The excitons photoexcited by the second laser pulse "probe" the excitons associated with the first laser pulse by way of recombination processes, thereby saturating the total amount of fluorescence collected from the film. Energy funneling dynamics can be time-resolved in layered perovskite systems because a significant amount of exciton−exciton annihilation occurs on the 100 ps time scale (see Figure 2d).[26]

In Figure 4, we present two-dimensional (2D) NLFL data acquired with a pair of color-tunable 300 fs laser pulses with 2 $\mu J/cm^2$ fluences and 4 nm spectral widths. The signals are acquired using the same experimental setup and conditions applied to films composed of larger quantum wells in ref 26. The present layered perovskite film, which is primarily a mixture of n = 2 and 3 quantum wells, exhibits the linear absorbance spectrum shown in Figure 3a. At a delay time of τ = 1 ps, the 2D NLFL spectrum possesses diagonal peaks (λ_1=λ_2) associated with the n = 2 and 3 quantum wells at 570 and 610 nm, respectively. These diagonal peaks represent a sequence in which the initially populated systems are probed with the second laser pulse before energy transfer occurs. In agreement with transient absorption data obtained for similar films,[39] the magnitude of a cross peak at λ_1 = 570 and λ_2 = 610 nm increases on the sub-ns time scale due to energy funneling processes.[39] Thus, although both pulses interact with quantum wells in their ground electronic states, the NLFL data reveal energy funneling dynamics by way of the recombination-induced mechanism illustrated in Figure 3c. Whereas transient absorption experiments conducted on layered perovskites reflect all energy funneling dynamics regardless of the terminal energy acceptors,[39] the NLFL spectra shown in Figure 4 are specific to relaxation processes that ultimately concentrate excitations in the thickest quantum wells because the signals are detected at 725 nm (see Figure 3b).

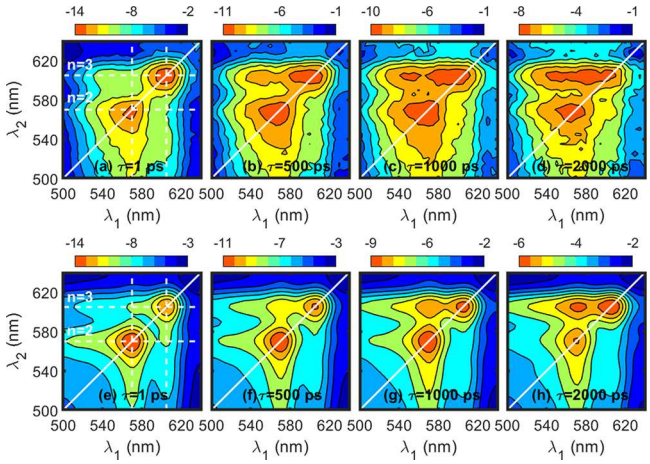

Figure 4. Experimental (a)−(d) and calculated (e)−(h) NLFL spectra are displayed for a layered perovskite system primarily composed of n = 2 and 3 quantum wells. Delay times of τ = 1, 500, 1000, and 2000 ps are specified in the respective panels. The experimental data exhibit broader line widths due to a pulse width-limited spectral resolution of 4 nm. Signals are expressed as percentages using eq 8. Detection of fluorescence at 725 nm makes the nonlinear response specific to processes that funnel energy into the thickest quantum wells.

To more rigorously demonstrate the information provided by recombination-induced nonlinearities, we calculate the 2D NLFL spectra in Figure 4e−h using parameters obtained from global fits of conventional transient absorption data (e.g., exciton resonance frequencies, energy transfer rates, lifetimes).[39] The exciton and higher energy continuum line shapes associated with the quantum wells are parametrized using experimental linear absorbance spectra acquired for pure-phase crystals, $A_n(\omega)$ (see the Supporting Information).[40] The exciton density in quantum well n at time-zero is given by

$$\sigma_n(\omega, \tau = 0) = \frac{f(\omega)}{\hbar\omega d}[1 - 10^{-c_n A_n(\omega)}] \tag{5}$$

where $f(\omega)$ is the laser fluence, ω is the frequency of the laser pulse, d is the film thickness, and c_n is the fraction of absorbance associated with quantum well n at frequency ω. The dynamics occurring in the experimentally controlled delay time, τ, are simulated using a system of differential equations developed for fitting transient absorption data:[39]

https://doi.org/10.1021/acs.jpcc.2c08851
J. Phys. Chem. C 2023, 127, 2782−2791

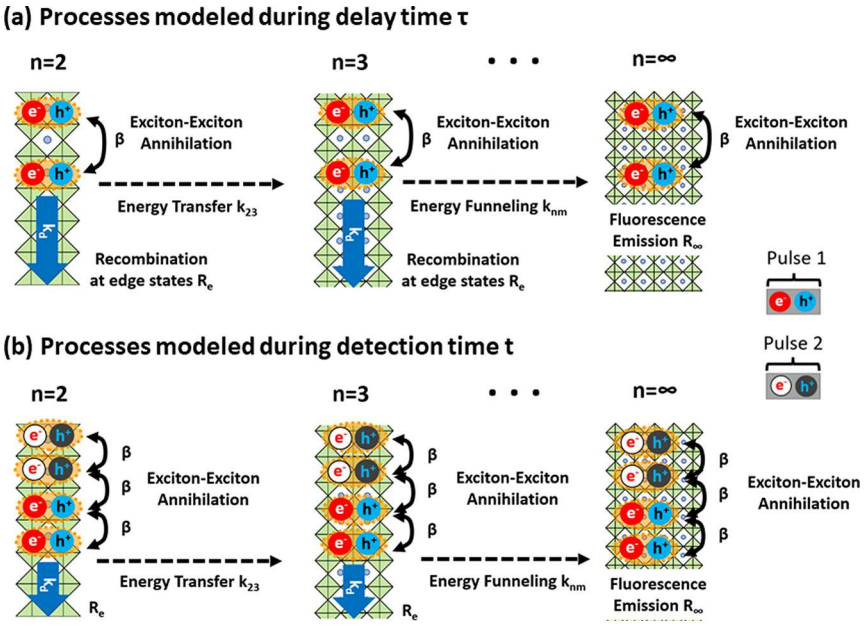

Figure 5. Summary of relaxations mechanisms modeled during the (a) experimentally controlled delay time τ and (b) detection time t. The NLFL response originates in annihilation processes associated with excitons photoexcited by separate laser pulses. Recombination-induced nonlinearities are problematic in Fourier transform action spectroscopies; however, the present measurements and calculations demonstrate that recombination can be leveraged for studies of transport mechanisms on nanosecond time scales.

$$\frac{\partial \sigma_n}{\partial \tau} = (-k_{n,n-1} - k_{n,n+1} - k_d - \beta\sigma_n)\sigma_n + k_{n-1,n}\sigma_{n-1} + k_{n+1,n}\sigma_{n+1},\quad n = 2\text{–}4$$

$$\frac{\partial \sigma_5}{\partial \tau} = (-k_{5,4} - k_{5,\infty} - k_d - \beta\sigma_5)\sigma_5 + k_{4,5}\sigma_5 + k_{\infty,5}\sigma_\infty$$

$$\frac{\partial \sigma_\infty}{\partial \tau} = (-k_{\infty,5} - R_\infty - \beta\sigma_\infty)\sigma_\infty + k_{5,\infty}\sigma_5$$

$$\frac{\partial \sigma_{ne}}{\partial \tau} = k_d\sigma_n - R_e\sigma_{ne},\ n = 2\text{–}5 \tag{6}$$

$$\frac{\partial \xi_n}{\partial t} = (-k_{n,n-1} - k_{n,n+1} - k_d - \beta\xi_n)\xi_n + k_{n-1,n}\xi_{n-1} + k_{n+1,n}\xi_{n+1},\quad n = 2\text{–}4$$

$$\frac{\partial \xi_5}{\partial t} = (-k_{5,4} - k_{5,\infty} - k_d - \beta\xi_5)\xi_5 + k_{4,5}\xi_5 + k_{\infty,5}\xi_\infty$$

$$\frac{\partial \xi_\infty}{\partial t} = (-k_{\infty,5} - R_\infty - \beta\xi_\infty)\xi_\infty + k_{5,\infty}\xi_5$$

$$\frac{\partial \xi_{ne}}{\partial t} = k_d\xi_n - R_e\xi_{ne},\ n = 2\text{–}5 \tag{7}$$

Briefly, k_{nm} is the rate constant for energy transfer from quantum well n to quantum well m (with reverse rates accounted for using detailed balance), β is the exciton−exciton annihilation coefficient, and R_∞ is the radiative recombination rate for the $n = \infty$ system. The model also accounts for defect-assisted recombination at "layer edge states."[55] The population, σ_{ne}, represents layer edge states in quantum well, n. The rate of diffusion to an edge state is given by k_d, whereas R_e represents recombination. Parameters of the model are illustrated with schematics in Figure 5.

The same processes occur in the delay time, τ, for both conventional transient absorption and NLFL experiments; however, calculations of the kinetics must be reinitiated during the signal detection time, t, in NLFL spectroscopy (see Figure 3c). The initial conditions in the detection time, t, are established by summing the exciton densities photoexcited by separate laser pulses using $\xi_n(\omega_1, \tau, \omega_2, t = 0) = \sigma_n(\omega_1, \tau) + \sigma_n(\omega_2, 0)$. The population of an edge state at $t = 0$ is written as $\xi_{ne}(\omega_1, \tau, \omega_2, t = 0) = \sigma_{ne}(\omega_1, \tau)$. The same system of equations is then solved during the detection time, t:

Energy is funneled to the $n = \infty$ system from which fluorescence is detected at 725 nm. Because the emission rate is proportional to the excited-state population of the $n = \infty$ quantum well, the NLFL signal (i.e., fraction of saturation in the response) measured at the delay time, τ, can be written as

$$\Phi_{\mathrm{NLFL}}(\omega_1, \tau, \omega_2) = \frac{\int_0^\infty [\xi_\infty(\omega_1, \tau, \omega_2, t) - \sigma_\infty(\omega_1, t) - \sigma_\infty(\omega_2, t)]\,\mathrm{d}t}{\int_0^\infty [\sigma_\infty(\omega_1, t) + \sigma_\infty(\omega_2, t)]\,\mathrm{d}t} \tag{8}$$

In Figures 4e–h, the NLFL spectra simulated using eq 8 capture the patterns of resonances in the 2D spectra, dynamics in the amount of signal saturation, and the time scales of energy funneling. The calculations are consistent with the schematics presented in Figure 5 in that energy funneling dynamics are revealed despite the "linear" natures of the field-matter interactions. The differences in the experimental and simulated NLFL data in Figure 4 likely originate from the 4 nm spectral resolution of the experiments and the complexities of the exciton and continuum contributions to the absorbance line shapes (see the Supporting Information).

https://doi.org/10.1021/acs.jpcc.2c08851
J. Phys. Chem. C 2023, 127, 2782−2791

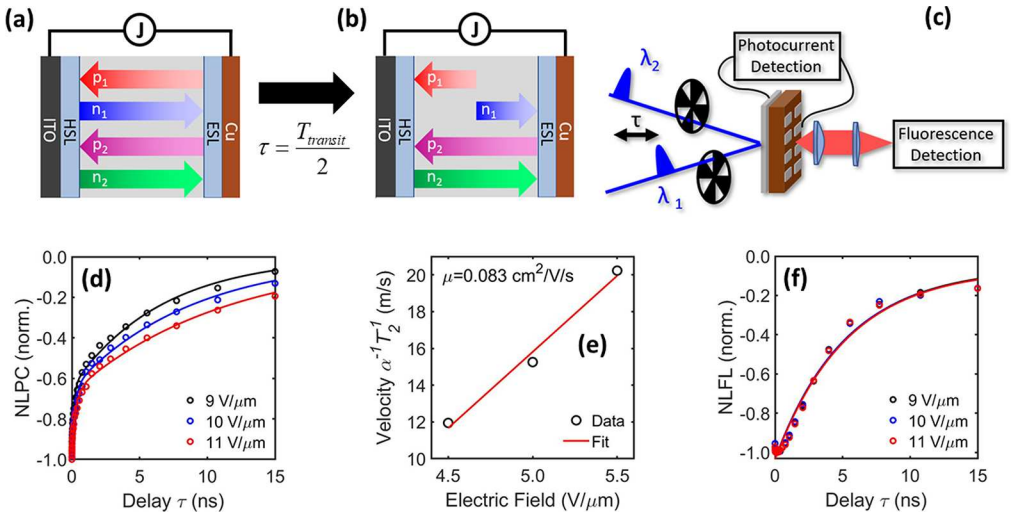

Figure 6. Method for distinguishing dynamics of excitons and free charge carriers in layered perovskite systems. Electrons and holes photoexcited by the first and second laser pulses drift in the directions indicated by the arrows at delay times of (a) $\tau = 0$ and (b) $\tau = T_{transit}/2$. (c) Nonlinear photocurrent and fluorescence signals are detected under the same experimental conditions. (d) NLPC signals are acquired at three potentials to vary the drift velocities. (e) The carrier mobility is obtained by fitting the drift velocities versus the electric fields to a straight line. These data represent an average of four data sets acquired with three separate devices. (f) Excitons dominate the fluorescence channel of the experiment and do not respond to the applied bias due to their neutral charges.

DISTINGUISHING EXCITONS AND FREE CHARGE CARRIERS WITH TANDEM NONLINEAR PHOTOCURRENT AND FLUORESCENCE SPECTROSCOPIES

In contrast to the spatially localized energy funneling dynamics revealed by the NLFL spectra in Figure 4, nonlinear photocurrent (NLPC) spectroscopies can be employed to study long-range carrier transport in photovoltaic cells.[28−30] In these approaches, the first laser pulse initiates carrier drift within the active layer of a device and recombination processes involving the carriers photoexcited by the second laser pulse enable resolution of the transit time. For example, the holes (p_k) and electrons (n_k) associated with pulse k (k = 1 or 2) are depicted in Figure 6a. The lengths of the arrows represent spatial distributions of the carrier densities (i.e., the darkest shades are most concentrated), whereas the directions reflect electric field-induced drift within the active layer. Transient absorption experiments suggest that the recombination processes in layered perovskite systems are primarily two-body in nature.[39,40,56] Thus, like the exciton−exciton annihilation dynamics discussed above, the recombination rates responsible for the nonlinearity in the photocurrent scale as the products of carrier densities photoexcited by separate laser pulses, $\beta p_1 n_2$ and $\beta n_1 p$.[29,30] The magnitude of the NLPC response decreases as the carrier densities, p_1 and n_1, drift from the illuminated region of the active layer and inject into the electrodes during the experimentally controlled delay time.

In recent works, we have presented several approaches for obtaining time-of-flight information with NLPC experiments.[27−30] The external biases are cycled in these techniques to probe the dynamics of free charges; however, excitons are the dominant electronically excited species in the present layered perovskite systems. The n = 2 and 3 quantum wells (i.e., the most concentrated systems in the present material) have exciton binding energies of approximately 251 and 177 meV, which suggests the numbers of excitons must greatly outweigh those of the free charge carriers.[57] For example, with these binding energies, Saha's equation predicts the percentages of free charge carriers are approximately 1.6 and 3.1% in the n = 2 and 3 quantum wells, respectively.[40] Whereas the contribution of free charge carriers to the photocurrent is unambiguous, fluorescence can originate from either excitons or radiative recombination of free charges. In addition to fundamental interest in excited state dynamics, knowledge of the species that contribute to lossy mechanisms in photovoltaic cells holds practical significance for optimizing materials.

The experimental setup depicted in Figure 6c can be used to distinguish contributions of excitons and free charges to the photocurrent and fluorescence produced by a device. An earlier version of this setup was employed to acquire 2D NLPC and NLFL spectra in ref 26; however, the delay time was limited to 3 ns and the potential was held constant in this work. Varying the external bias improves the ability to distinguish excitons and free carriers because (neutral) excitons do not drift under the influence of the electric field applied across the active layer. In contrast, the drift velocity for free charges is given by $v_{drift} = \mu \cdot V/d$, where V is the experimentally controlled potential, μ is the carrier mobility, and d is the active layer thickness.

The NLPC data presented in Figure 6d demonstrate that the decay times decrease as the magnitudes of the electric fields increase due to concomitant increases in the drift velocities. In our experience, NLPC decay profiles involving small quantum wells typically exhibit a sub-ns phase of nonradiative decay, which we refer to as T_1, followed by a ∼10 ns phase of carrier drift, T_2.[27−29] To extract carrier transit times, the signals in Figure 6d are fit to sums of exponential functions:

$$S(\tau) = A_1 \exp(-\tau/T_1) + A_2 \exp(-\tau/T_2) \quad (9)$$

The drift velocities are then computed using $v_{drift} = \alpha^{-1}T_2^{-1}$, where α is the 7.48 μm^{-1} absorption coefficient of the film with 570 nm incident light (see the Supporting Information). With inspiration from conventional time-of-flight methods,[58,59] the potential is varied to extract a carrier mobility of μ = 0.083 ± 0.010 $cm^3/V/s$ from the data sets presented in Figure 6e.[27−30] Here, the uncertainty of 0.010 $cm^3/V/s$ in the mobility is the

https://doi.org/10.1021/acs.jpcc.2c08851
J. Phys. Chem. C 2023, 127, 2782−2791

standard error of the regression slope for the three points shown in Figure 6e. To account for the variability in fabrication conditions, these three velocities represent averages computed with four data sets acquired using three separate photovoltaic cells (see Supporting Information). Unlike the NLPC signals, the NLFL decay profiles shown in Figure 6f are independent of the electric field which suggests that excitons dominate fluorescence emission for this material.

Free charge carriers represent less than 5% of the photoexcited species in the present layered perovskite systems because of large exciton binding energies; however, we suggest that tandem NLPC and NLFL experiments may be leveraged to distinguish excitons and free charges in materials where species coexist in a wider range of proportions. For example, as the thicknesses of layered perovskite quantum wells increase, the relative concentrations of excitons and free charges decrease and increase, respectively, due to weakening of the exciton binding energies.[57] Knowledge of the photoexcited species is essential for understanding transport mechanisms in layered perovskite materials because parallel energy and charge funneling processes are initiated by light absorption;[26,60] however, coexisting excitons and free charge carriers are also found in three-dimensional perovskites. For example, long-range order in $MAPbI_3$ nanocrystals boosts exciton stabilities, whereas free carrier populations dominate smaller domains in solution-processed films.[61,62] Although characterizations of perovskite light harvesting materials can be challenged by the presence of both excitons and free charges, tandem NLPC and NLFL experiments are equipped to decompose the species responsible for productive and lossy fluorescence processes within photovoltaic cells.

CONCLUDING REMARKS

In contrast to conventional nonlinear optical spectroscopies, the action spectroscopies described in this work exploit recombination-induced nonlinearities to probe transport mechanisms in photovoltaic cells. Alternate four-pulse action spectroscopies offer superior time resolution and reveal spectroscopic transitions between excited states, which are critically important for studies of femtosecond dynamics; however, such four-pulse Fourier transform methods are considerably more challenging and expensive to implement than the two-pulse approaches demonstrated in the present work (see Figure 1). Action spectroscopies involving recombination-induced nonlinear responses are well-suited for studies of nanosecond processes such as energy funneling in layered perovskite films and long-range drift in photovoltaic cells based on a variety of materials. In our experience, NLFL and NLPC spectroscopies can be successfully applied to materials with two-body recombination coefficients on the order of $\beta = 10^{-9}$ cm^3/s with laser fluences of 1−10 μJ/cm^2 (see Figure 2e). In addition to ease of implementation, the signals measured in recombination-induced action spectroscopies are generally 10^2−10^3 times greater than those associated with higher order perturbative responses in perovskite materials.[34] For these reasons, we suggest that the optimal experimental approach depends on the application and time scale of interest.

Although signal generation mechanisms are the primary emphasis of this work, the potential for conducting nonlinear action spectroscopies with low-cost picosecond diode lasers is a significant practical advantage when nanosecond processes are under investigation. In addition to affordability, the delay times between pulses generated by picosecond diode lasers are readily controlled with sub-30 ps precision using electronics. For example, we have recently conducted NLPC experiments using 40 ps diode lasers in which the delay time between pulses is scanned over a 100 ns range.[30] Whereas a mechanical delay line constrained the delay to 15 ns in Figure 6, the time interval between pulses is limited only by the repetition rate in an instrument employing picosecond diode lasers (e.g., delay times up to 1 ms are accessible at 1 kHz). Picosecond diode lasers with either fixed or continuum spectra may be employed in recombination-induced action spectroscopies depending on the desired information. In principle, 2D representations of the signals such as those shown in Figure 4 can be obtained with a picosecond continuum light source, thereby avoiding the complexities of a setup based on a femtosecond laser system. Development of affordable and low-maintenance instruments will make these practical techniques accessible to non-specialists.

ASSOCIATED CONTENT

Supporting Information

The Supporting Information is available free of charge at https://pubs.acs.org/doi/10.1021/acs.jpcc.2c08851.

We present further details regarding the numerical model used to calculate NLFL spectra in addition to all NLPC and NLFL data sets that contribute to the averaged signals shown in Figures 4 and 5. With 570 nm incident light, the 130 nm light penetration depth of the layered perovskite film is demonstrated with an SEM image and absorbance spectrum measured for a photovoltaic cell (PDF)

AUTHOR INFORMATION

Corresponding Author

Andrew M. Moran − *Department of Chemistry, University of North Carolina at Chapel Hill, Chapel Hill, North Carolina 27599, United States;* orcid.org/0000-0001-7761-7613; Email: ammoran@email.unc.edu

Authors

Meredith G. McNamee − *Department of Chemistry, University of North Carolina at Chapel Hill, Chapel Hill, North Carolina 27599, United States;* orcid.org/0000-0003-4432-5870

Zhenyu Ouyang − *Department of Chemistry, University of North Carolina at Chapel Hill, Chapel Hill, North Carolina 27599, United States;* orcid.org/0000-0001-9549-0353

Liang Yan − *Department of Chemistry, University of North Carolina at Chapel Hill, Chapel Hill, North Carolina 27599, United States;* orcid.org/0000-0003-4122-7466

Zijian Gan − *Department of Chemistry, University of North Carolina at Chapel Hill, Chapel Hill, North Carolina 27599, United States;* orcid.org/0000-0002-3751-5249

Ninghao Zhou − *Shanghai Huawei Technologies Co., Ltd., Shanghai 200120, China;* orcid.org/0000-0002-7255-282X

Olivia F. Williams − *Edmund Optics, Inc., Barrington, New Jersey 08007, United States;* orcid.org/0000-0001-5364-7703

Wei You − *Department of Chemistry, University of North Carolina at Chapel Hill, Chapel Hill, North Carolina 27599, United States;* orcid.org/0000-0003-0354-1948

Complete contact information is available at:
https://pubs.acs.org/10.1021/acs.jpcc.2c08851

Author Contributions

#M.G.M. and Z.O. contributed equally to this work.

Notes

The authors declare no competing financial interest.

Biographies

Meredith McNamee received a B.S. in Chemistry from North Carolina State University (Raleigh, NC) in 2019. He is a graduate student in Prof. Moran's group in the Department of Chemistry at the University of North Carolina at Chapel Hill and focuses on developing spectroscopic methods to probe layered perovskite devices.

Zhenyu Ouyang received his B.S. in Chemistry from the University of Science and Technology of China (Hefei, China) in 2018. He is currently a graduate student working in Prof. Andrew Moran's group in the Department of Chemistry at the University of North Carolina at Chapel Hill. His research focuses on the development of action spectroscopies for investigations of solar cell devices.

Liang Yan obtained his B.S. degree in Polymer Science and Engineering at Tsinghua University, Beijing, in 2003, and his M.S. degree in Material Science at Tsinghua University, Beijing, in 2006. He received his Ph.D. degree from Prof. Bin Hu's group in Materials Science and Engineering at the University of Tennessee at Knoxville in 2011. After that he started to work in Prof. Wei You's group as a Postdoctoral Research Associate and now as a Research Associate in the Department of Chemistry at the University of North Carolina at Chapel Hill. His research focused on organic solar cell and low-dimensional organic−inorganic hybrid perovskites.

Zijian Gan received his B.S. in Chemistry from the University of Science and Technology of China (Hefei, China) in 2022. He is currently a graduate student in Prof. Andrew Moran's group in the Department of Chemistry at the University of North Carolina at Chapel Hill. His research interests include the development of nonlinear spectroscopic techniques to study optoelectronic devices.

Ninghao Zhou received his B.S. in chemistry from the University of Science and Technology of China in 2016. He earned his Ph.D. under the supervision of Prof. Andrew Moran at the University of North Carolina Chapel Hill in 2021. Ninghao joined Shanghai Huawei Technologies Co., Ltd. as a senior engineer in 2022. His research interests focus on studying ultrafast dynamics in condensed-phase materials by nonlinear spectroscopic techniques.

Olivia Williams earned her Ph.D. in physical chemistry from the University of North Carolina at Chapel Hill in Prof. Andrew Moran's research group, where her research involved the use of transient absorption microscopies to study carrier dynamics and exciton transport in semiconductor materials. After her postdoctoral training under Prof. Libai Huang at Purdue University, Olivia joined Edmund Optics in late 2021 as an Ultrafast Laser Optics Engineer. In this role, she develops ultrafast optical solutions for customers working in numerous application spaces.

Wei You received his B.S. degree in Polymer Chemistry from University of Science and Technology of China (USTC) in 1999 and obtained his Ph.D. in 2004 under the guidance of Professor Luping Yu. He then moved west and finished his postdoctoral training at Stanford University in 2006 with Professor Zhenan Bao. In July 2006, Dr. You joined the University of North Carolina at Chapel Hill as an Assistant Professor in Chemistry and was promoted to the rank of Associate Professor in 2012 and then Full Professor in 2017. His research group focuses on (a) developing and fundamental understanding of novel materials for solar energy utilizations and (b) new polymeric materials based on novel polymerization methodologies for a variety of applications.

Andrew Moran earned a Ph.D. in Physical Chemistry from Kansas State University in 2002 under the direction of Professor Anne Myers Kelley. He then conducted research as a postdoctoral scholar with Professors Shaul Mukamel (University of Rochester), Kenneth Spears (Northwestern University), and Norbert Scherer (University of Chicago). Andrew arrived at the University of North Carolina in 2007 and is now a Full Professor. Andrew's research group uses nonlinear optical and action spectroscopies to investigate carrier transport processes in photovoltaic materials.

■ ACKNOWLEDGMENTS

This work is supported by the National Science Foundation under CHE-1763207 (M.M., Z.O., N.Z., O.W., and A.M.). L.Y. and W.Y. acknowledge support from the UNC Research Opportunities Initiative (ROI) through the Center of Hybrid Materials Enabled Electronic Technology. Research of 2D perovskites fabrication was supported by the Center for Hybrid Organic Inorganic Semiconductors for Energy (CHOISE), an Energy Frontier Research Center funded by the U.S. Department of Energy (DOE), Office of Science, Office of Basic Energy Sciences (BES). This work was performed in part at the Chapel Hill Analytical and Nanofabrication Laboratory, CHANL, a member of the North Carolina Research Triangle Nanotechnology Network, RTNN, which is supported by the National Science Foundation, Grant ECCS-2025064, as part of the National Nanotechnology Coordinated Infrastructure, NNCI.

■ REFERENCES

(1) Brixner, T.; Stenger, J.; Vaswani, H. M.; Cho, M.; Blankenship, R. E.; Fleming, G. R. Two-Dimensional Spectroscopy of Electronic Couplings in Photosynthesis. *Nature* **2005**, *434* (7033), 625−628.
(2) Ogilvie, J. P.; Kubarych, K. J. Chapter 5 Multidimensional Electronic and Vibrational Spectroscopy: An Ultrafast Probe of Molecular Relaxation and Reaction Dynamics. In *Advances in Atomic, Molecular, and Optical Physics*; Academic Press: 2009; Vol. *57*, pp 249−321.
(3) Jonas, D. M. Two-Dimensional Femtosecond Spectroscopy. *Annu. Rev. Phys. Chem.* **2003**, *54* (1), 425−463.
(4) Tian, P.; Keusters, D.; Suzaki, Y.; Warren, W. S. Femtosecond Phase-Coherent Two-Dimensional Spectroscopy. *Science* **2003**, *300* (5625), 1553−1555.
(5) Tekavec, P. F.; Lott, G. A.; Marcus, A. H. Fluorescence-Detected Two-Dimensional Electronic Coherence Spectroscopy by Acousto-Optic Phase Modulation. *J. Chem. Phys.* **2007**, *127* (21), 214307.
(6) Schröter, M.; Pullerits, T.; Kühn, O. Using Fluorescence Detected Two-Dimensional Spectroscopy to Investigate Initial Exciton Delocalization between Coupled Chromophores. *J. Chem. Phys.* **2018**, *149* (11), 114107.
(7) Tiwari, V.; Matutes, Y. A.; Gardiner, A. T.; Jansen, T. L. C.; Cogdell, R. J.; Ogilvie, J. P. Spatially-Resolved Fluorescence-Detected Two-Dimensional Electronic Spectroscopy Probes Varying Excitonic Structure in Photosynthetic Bacteria. *Nat. Commun.* **2018**, *9* (1), 4219.
(8) Tiwari, V.; Matutes, Y. A.; Konar, A.; Yu, Z.; Ptaszek, M.; Bocian, D. F.; Holten, D.; Kirmaier, C.; Ogilvie, J. P. Strongly Coupled Bacteriochlorin Dyad Studied Using Phase-Modulated Fluorescence-Detected Two-Dimensional Electronic Spectroscopy. *Opt. Express* **2018**, *26* (17), 22327−22341.
(9) Kalaee, A. A. S.; Damtie, F.; Karki, K. J. Differentiation of True Nonlinear and Incoherent Mixing of Linear Signals in Action-

Detected 2d Spectroscopy. *J. Phys. Chem. A* **2019**, *123* (19), 4119−4124.
(10) Karki, K. J.; Chen, J.; Sakurai, A.; Shi, Q.; Gardiner, A. T.; Kühn, O.; Cogdell, R. J.; Pullerits, T. Before Förster. Initial Excitation in Photosynthetic Light Harvesting. *Chemical Science* **2019**, *10* (34), 7923−7928.
(11) Kunsel, T.; Tiwari, V.; Matutes, Y. A.; Gardiner, A. T.; Cogdell, R. J.; Ogilvie, J. P.; Jansen, T. L. C. Simulating Fluorescence-Detected Two-Dimensional Electronic Spectroscopy of Multichromophoric Systems. *J. Phys. Chem. B* **2019**, *123* (2), 394−406.
(12) Kühn, O.; Mančal, T.; Pullerits, T. Interpreting Fluorescence Detected Two-Dimensional Electronic Spectroscopy. *J. Phys. Chem. Lett.* **2020**, *11* (3), 838−842.
(13) Mueller, S.; Brixner, T. Molecular Coherent Three-Quantum Two-Dimensional Fluorescence Spectroscopy. *J. Phys. Chem. Lett.* **2020**, *11* (13), 5139−5147.
(14) Malý, P.; Mueller, S.; Lüttig, J.; Lambert, C.; Brixner, T. Signatures of Exciton Dynamics and Interaction in Coherently and Fluorescence-Detected Four- and Six-Wave-Mixing Two-Dimensional Electronic Spectroscopy. *J. Chem. Phys.* **2020**, *153* (14), 144204.
(15) Ouyang, Z.; Zhou, N.; Hu, J.; Williams, O. F.; Yan, L.; You, W.; Moran, A. M. Nonlinear Fluorescence Spectroscopy of Layered Perovskite Quantum Wells. *J. Chem. Phys.* **2020**, *153* (13), 134202.
(16) Agathangelou, D.; Javed, A.; Sessa, F.; Solinas, X.; Joffre, M.; Ogilvie, J. P. Phase-Modulated Rapid-Scanning Fluorescence-Detected Two-Dimensional Electronic Spectroscopy. *J. Chem. Phys.* **2021**, *155* (9), 094201.
(17) Heussman, D.; Kittell, J.; von Hippel, P. H.; Marcus, A. H. Temperature-Dependent Local Conformations and Conformational Distributions of Cyanine Dimer Labeled Single-Stranded−Double-Stranded DNA Junctions by 2d Fluorescence Spectroscopy. *J. Chem. Phys.* **2022**, *156* (4), 045101.
(18) Lanzani, G.; Zenz, C.; Cerullo, G.; Graupner, W.; Leising, G.; Scherf, U.; De Silvestri, S. Femtosecond Photovoltage Excitation Cross-Correlation on a Ladder-Type Polymer. *Synth. Met.* **2000**, *111−112*, 493−496.
(19) Müller, J. G.; Scherf, U.; Lemmer, U. Two Step Charge Carrier Generation in a Ladder-Type Conjugated Polymer. *Synth. Met.* **2001**, *119* (1), 395−396.
(20) Bakulin, A. A.; Rao, A.; Pavelyev, V. G.; van Loosdrecht, P. H. M.; Pshenichnikov, M. S.; Niedzialek, D.; Cornil, J.; Beljonne, D.; Friend, R. H. The Role of Driving Energy and Delocalized States for Charge Separation in Organic Semiconductors. *Science* **2012**, *335* (6074), 1340.
(21) Nardin, G.; Autry, T. M.; Silverman, K. L.; Cundiff, S. T. Multidimensional Coherent Photocurrent Spectroscopy of a Semiconductor Nanostructure. *Opt. Express* **2013**, *21* (23), 28617−28627.
(22) Karki, K. J.; Widom, J. R.; Seibt, J.; Moody, I.; Lonergan, M. C.; Pullerits, T.; Marcus, A. H. Coherent Two-Dimensional Photocurrent Spectroscopy in a Pbs Quantum Dot Photocell. *Nat. Commun.* **2014**, *5* (1), 5869.
(23) Bakulin, A. A.; Silva, C.; Vella, E. Ultrafast Spectroscopy with Photocurrent Detection: Watching Excitonic Optoelectronic Systems at Work. *J. Phys. Chem. Lett.* **2016**, *7* (2), 250−258.
(24) Vella, E.; Li, H.; Grégoire, P.; Tuladhar, S. M.; Vezie, M. S.; Few, S.; Bazán, C. M.; Nelson, J.; Silva-Acuña, C.; Bittner, E. R. Ultrafast Decoherence Dynamics Govern Photocarrier Generation Efficiencies in Polymer Solar Cells. *Sci. Rep.* **2016**, *6* (1), 29437.
(25) Bolzonello, L.; Bernal-Texca, F.; Gerling, L. G.; Ockova, J.; Collini, E.; Martorell, J.; van Hulst, N. F. Photocurrent-Detected 2d Electronic Spectroscopy Reveals Ultrafast Hole Transfer in Operating Pm6/Y6 Organic Solar Cells. *J. Phys. Chem. Lett.* **2021**, *12* (16), 3983−3988.
(26) Zhou, N.; Ouyang, Z.; Hu, J.; Williams, O. F.; Yan, L.; You, W.; Moran, A. M. Distinguishing Energy- and Charge-Transfer Processes in Layered Perovskite Quantum Wells with Two-Dimensional Action Spectroscopies. *J. Phys. Chem. Lett.* **2020**, *11* (12), 4570−4577.
(27) Zhou, N.; Ouyang, Z.; Yan, L.; McNamee, M. G.; You, W.; Moran, A. M. Elucidation of Quantum-Well-Specific Carrier Mobilities in Layered Perovskites. *J. Phys. Chem. Lett.* **2021**, *12* (4), 1116−1123.
(28) Ouyang, Z.; Zhou, N.; McNamee, M. G.; Yan, L.; Williams, O. F.; You, W.; Moran, A. M. Multidimensional Time-of-Flight Spectroscopy. *J. Chem. Phys.* **2021**, *154* (22), 220901.
(29) Ouyang, Z.; Zhou, N.; McNamee, M. G.; Yan, L.; Williams, O. F.; Gan, Z.; Gao, R.; You, W.; Moran, A. M. Origin of Layered Perovskite Device Efficiencies Revealed by Multidimensional Time-of-Flight Spectroscopy. *J. Chem. Phys.* **2022**, *156* (8), 084202.
(30) Ouyang, Z.; Yan, L.; You, W.; Moran, A. M. Probing Drift Velocity Dispersion in Mapbi3 Photovoltaic Cells with Nonlinear Photocurrent Spectroscopy. *J. Chem. Phys.* **2022**, *157* (17), 174202.
(31) Mastron, J. N.; Tokmakoff, A. Fourier Transform Fluorescence-Encoded Infrared Spectroscopy. *J. Phys. Chem. A* **2018**, *122* (2), 554−562.
(32) Mukamel, S. *Principles of Nonlinear Optical Spectroscopy*; Oxford University Press: New York, 1995.
(33) Landsberg, P. T. *Recombination in Semiconductors*; Cambridge University Press: Cambridge, 1991.
(34) Grégoire, P.; Srimath Kandada, A. R.; Vella, E.; Tao, C.; Leonelli, R.; Silva, C. Incoherent Population Mixing Contributions to Phase-Modulation Two-Dimensional Coherent Excitation Spectra. *J. Chem. Phys.* **2017**, *147* (11), 114201.
(35) Damtie, F. A.; Wacker, A.; Pullerits, T.; Karki, K. J. Two-Dimensional Action Spectroscopy of Excitonic Systems: Explicit Simulation Using a Phase-Modulation Technique. *Phys. Rev. A* **2017**, *96* (5), 053830.
(36) Bargigia, I.; Gutiérrez-Meza, E.; Valverde-Chávez, D. A.; Marques, S. R.; Srimath Kandada, A. R.; Silva, C. Identifying Incoherent Mixing Effects in the Coherent Two-Dimensional Photocurrent Excitation Spectra of Semiconductors. *J. Chem. Phys.* **2022**, *157* (20), 204202.
(37) Blank, D. A.; Kaufman, L. J.; Fleming, G. R. Fifth-Order Two-Dimensional Raman Spectra of Cs2 Are Dominated by Third-Order Cascades. *J. Chem. Phys.* **1999**, *111* (7), 3105−3114.
(38) Kubarych, K. J.; Milne, C. J.; Miller, R. J. D. Fifth-Order Two-Dimensional Raman Spectroscopy: A New Direct Probe of the Liquid State. *Int. Rev. Phys. Chem.* **2003**, *22* (3), 497−532.
(39) Williams, O. F.; Guo, Z.; Hu, J.; Yan, L.; You, W.; Moran, A. M. Energy Transfer Mechanisms in Layered 2d Perovskites. *J. Chem. Phys.* **2018**, *148* (13), 134706.
(40) Williams, O. F.; Zhou, N.; Hu, J.; Ouyang, Z.; Kumbhar, A.; You, W.; Moran, A. M. Imaging Excited State Dynamics in Layered 2d Perovskites with Transient Absorption Microscopy. *J. Phys. Chem. A* **2019**, *123* (51), 11012−11021.
(41) Xiao, X.; Wu, M.; Ni, Z.; Xu, S.; Chen, S.; Hu, J.; Rudd, P. N.; You, W.; Huang, J. Ultrafast Exciton Transport with a Long Diffusion Length in Layered Perovskites with Organic Cation Functionalization. *Adv. Mater.* **2020**, *32* (46), 2004080.
(42) Deng, S.; Shi, E.; Yuan, L.; Jin, L.; Dou, L.; Huang, L. Long-Range Exciton Transport and Slow Annihilation in Two-Dimensional Hybrid Perovskites. *Nat. Commun.* **2020**, *11* (1), 664.
(43) Spitha, N.; Kohler, D. D.; Hautzinger, M. P.; Li, J.; Jin, S.; Wright, J. C. Discerning between Exciton and Free-Carrier Behaviors in Ruddlesden−Popper Perovskite Quantum Wells through Kinetic Modeling of Photoluminescence Dynamics. *J. Phys. Chem. C* **2020**, *124* (31), 17430−17439.
(44) Herz, L. M. Charge-Carrier Dynamics in Organic-Inorganic Metal Halide Perovskites. *Annu. Rev. Phys. Chem.* **2016**, *67* (1), 65−89.
(45) Manser, J. S.; Kamat, P. V. Band Filling with Free Charge Carriers in Organometal Halide Perovskites. *Nat. Photonics* **2014**, *8* (9), 737−743.
(46) Cao, D. H.; Stoumpos, C. C.; Farha, O. K.; Hupp, J. T.; Kanatzidis, M. G. 2d Homologous Perovskites as Light-Absorbing Materials for Solar Cell Applications. *J. Am. Chem. Soc.* **2015**, *137* (24), 7843−7850.
(47) Stoumpos, C. C.; Cao, D. H.; Clark, D. J.; Young, J.; Rondinelli, J. M.; Jang, J. I.; Hupp, J. T.; Kanatzidis, M. G. Ruddlesden−Popper

https://doi.org/10.1021/acs.jpcc.2c08851
J. Phys. Chem. C 2023, 127, 2782−2791

Hybrid Lead Iodide Perovskite 2d Homologous Semiconductors. *Chem. Mater.* **2016**, *28* (8), 2852−2867.
(48) Yuan, M.; Quan, L. N.; Comin, R.; Walters, G.; Sabatini, R.; Voznyy, O.; Hoogland, S.; Zhao, Y.; Beauregard, E. M.; Kanjanaboos, P.; Lu, Z.; Kim, D. H.; Sargent, E. H. Perovskite Energy Funnels for Efficient Light-Emitting Diodes. *Nat. Nanotechnol.* **2016**, *11* (10), 872−877.
(49) Yan, L.; Hu, J.; Guo, Z.; Chen, H.; Toney, M. F.; Moran, A. M.; You, W. General Post-Annealing Method Enables High-Efficiency Two-Dimensional Perovskite Solar Cells. *ACS Appl. Mater. Interfaces* **2018**, *10* (39), 33187−33197.
(50) Zheng, K.; Chen, Y.; Sun, Y.; Chen, J.; Chábera, P.; Schaller, R.; Al-Marri, M. J.; Canton, S. E.; Liang, Z.; Pullerits, T. Inter-Phase Charge and Energy Transfer in Ruddlesden−Popper 2d Perovskites: Critical Role of the Spacing Cations. *Journal of Materials Chemistry A* **2018**, *6* (15), 6244−6250.
(51) Mauck, C. M.; Tisdale, W. A. Excitons in 2d Organic−Inorganic Halide Perovskites. *Trends Chem.* **2019**, *1*, 380−393.
(52) Proppe, A. H.; Elkins, M. H.; Voznyy, O.; Pensack, R. D.; Zapata, F.; Besteiro, L. V.; Quan, L. N.; Quintero-Bermudez, R.; Todorovic, P.; Kelley, S. O.; Govorov, A. O.; Gray, S. K.; Infante, I.; Sargent, E. H.; Scholes, G. D. Spectrally Resolved Ultrafast Exciton Transfer in Mixed Perovskite Quantum Wells. *J. Phys. Chem. Lett.* **2019**, *10* (3), 419−426.
(53) Lei, L.; Seyitliyev, D.; Stuard, S.; Mendes, J.; Dong, Q.; Fu, X.; Chen, Y.-A.; He, S.; Yi, X.; Zhu, L.; Chang, C.-H.; Ade, H.; Gundogdu, K.; So, F. Efficient Energy Funneling in Quasi-2d Perovskites: From Light Emission to Lasing. *Adv. Mater.* **2020**, *32* (16), 1906571.
(54) Panuganti, S.; Besteiro, L. V.; Vasileiadou, E. S.; Hoffman, J. M.; Govorov, A. O.; Gray, S. K.; Kanatzidis, M. G.; Schaller, R. D. Distance Dependence of Förster Resonance Energy Transfer Rates in 2d Perovskite Quantum Wells Via Control of Organic Spacer Length. *J. Am. Chem. Soc.* **2021**, *143* (11), 4244−4252.
(55) Blancon, J. C.; Tsai, H.; Nie, W.; Stoumpos, C. C.; Pedesseau, L.; Katan, C.; Kepenekian, M.; Soe, C. M. M.; Appavoo, K.; Sfeir, M. Y.; Tretiak, S.; Ajayan, P. M.; Kanatzidis, M. G.; Even, J.; Crochet, J. J.; Mohite, A. D. Extremely Efficient Internal Exciton Dissociation through Edge States in Layered 2d Perovskites. *Science* **2017**, *355* (6331), 1288−1292.
(56) Guo, Z.; Zhou, N.; Williams, O. F.; Hu, J.; You, W.; Moran, A. M. Imaging Carrier Diffusion in Perovskites with a Diffractive Optic-Based Transient Absorption Microscope. *J. Phys. Chem. C* **2018**, *122* (19), 10650−10656.
(57) Blancon, J. C.; Stier, A. V.; Tsai, H.; Nie, W.; Stoumpos, C. C.; Traoré, B.; Pedesseau, L.; Kepenekian, M.; Katsutani, F.; Noe, G. T.; Kono, J.; Tretiak, S.; Crooker, S. A.; Katan, C.; Kanatzidis, M. G.; Crochet, J. J.; Even, J.; Mohite, A. D. Scaling Law for Excitons in 2d Perovskite Quantum Wells. *Nat. Commun.* **2018**, *9* (1), 2254.
(58) Bronger, T. Time-of-Flight Analysis. In *Advanced Characterization Techniques for Thin Film Solar Cells*; Abou-Ras, D., Kirchartz, T., Rau, U.,, Eds.; Wiley-VCH: Weinheim, 1991; Vol. *1*, pp 121−145.
(59) Dong, Q.; Fang, Y.; Shao, Y.; Mulligan, P.; Qiu, J.; Cao, L.; Huang, J. Electron-Hole Diffusion Lengths > 175 Mm in Solution-Grown Ch3nh3pbi3 Single Crystals. *Science* **2015**, *347* (6225), 967.
(60) Liu, J.; Leng, J.; Wu, K.; Zhang, J.; Jin, S. Observation of Internal Photoinduced Electron and Hole Separation in Hybrid Two-Dimentional Perovskite Films. *J. Am. Chem. Soc.* **2017**, *139* (4), 1432−1435.
(61) Nah, S.; Spokoyny, B.; Stoumpos, C.; Soe, C. M. M.; Kanatzidis, M.; Harel, E. Spatially Segregated Free-Carrier and Exciton Populations in Individual Lead Halide Perovskite Grains. *Nat. Photonics* **2017**, *11* (5), 285−288.
(62) Grancini, G.; Srimath Kandada, A. R.; Frost, J. M.; Barker, A. J.; De Bastiani, M.; Gandini, M.; Marras, S.; Lanzani, G.; Walsh, A.; Petrozza, A. Role of Microstructure in the Electron−Hole Interaction of Hybrid Lead Halide Perovskites. *Nat. Photonics* **2015**, *9* (10), 695−701.

https://doi.org/10.1021/acs.jpcc.2c08851
J. Phys. Chem. C 2023, 127, 2782−2791